Available online at www.sciencedirect.com
SCIENCE DIRECT®
Journal of Solid State Chemistry 178 (2005) 1851–1863
JOURNAL OF SOLID STATE CHEMISTRY
www.elsevier.com/locate/jssc

Crystal structures, physical properties and NMR experiments on the ternary rare-earth metal silicide boride compounds $RE_5Si_2B_8$ (RE = Y, Sm, Gd, Tb, Dy, Ho)

Jérome Roger[a], Volodymyr Babizhetskyy[a,b], Stéphane Cordier[a], Josef Bauer[a], Kurt Hiebl[c], Laurent Le Pollès[a], Sharon Elisabeth Ashbrook[d], Jean-François Halet[a], Roland Guérin[a,*]

[a]*Laboratoire de Chimie du Solide et Inorganique Moléculaire, UMR CNRS 6511, Université de Rennes 1-ENSCR, Institut de Chimie, Campus de Beaulieu, Avenue du Général Leclerc, F-35042 Rennes, Cedex, France*
[b]*Max-Planck-Institute für Festkörperforschung, Heisenbergstrasse 1, Postfach 800665, D-70569 Stuttgart, Germany*
[c]*Institut für Physikalische Chemie, Universität Wien, Währingerstrasse 42, A-1090 Wien, Austria*
[d]*Department of Earth Sciences, University of Cambridge, Downing Street, Cambridge CB2 3EQ, UK*

Received 4 January 2005; received in revised form 23 February 2005; accepted 27 February 2005
Available online 18 April 2005

Abstract

The ternary rare-earth metal silicide borides $RE_5Si_2B_8$ (RE = Y, Sm, Gd, Tb, Dy Ho) were prepared by arc melting the elemental components and subsequent annealing up to $T = 1850$ K. The crystal structure was determined for each term of the series from single-crystal X-ray data: tetragonal symmetry, space group $P4/mbm$, $Z = 2$; unit cell parameters $a = 7.2616(3)$, $c = 8.2260(3)$ Å and $a = 7.1830(2)$, $c = 7.9900(3)$ Å for $Sm_5Si_2B_8$ and $Ho_5Si_2B_8$, respectively. The structure is a new type and can be structurally described as an intergrowth of ThB_4-like and U_3Si_2-like slabs of composition REB_4 and RE_3Si_2, respectively, alternating along the c direction. The boron and silicon substructures are wholly independent and well ordered. The magnetic properties are as follows: $Y_5Si_2B_8$ is a Pauli-type paramagnet above 1.8 K, $Gd_5Si_2B_8$ undergoes a weak (canted) ferromagnetic-like order at 70 K followed by a colinear antiferromagnetic spin alignment at 44 K. $Tb_5Si_2B_8$ and $Dy_5Si_2B_8$ order antiferromagnetically at a Néel temperature of $T_N = 45$ and 28 K, respectively. In the paramagnetic regime, the effective moments are in good accord with the theoretical RE^{3+} free ion moments. The temperature dependence of the electrical resistivities for the Y, Gd, Tb, and Dy containing samples corroborates with the metallic state of the nonmagnetic (Y) and the magnetically ordered compounds. ^{11}B, ^{29}Si and ^{89}Y nuclear magnetic resonance (NMR) spectroscopy on nonmagnetic $Y_5Si_2B_8$ shows different signals, which correspond to the expected number of distinct crystallographic sites in the structure. ^{11}B NMR on $Y_5Si_2B_8$ indicates that the local magnetic susceptibilities are substantially different from the ones observed in the related compound YB_4.

Keywords: Rare-earth metal silicide boride; Crystal structure; Magnetic behavior; Electrical resistivity; NMR spectroscopy

1. Introduction

Binary rare-earth (RE) metal borides and silicides have been extensively studied and exhibit a rich structural chemistry. In contrast, the combination of boron and silicon with RE metals has been poorly investigated and ternary silicide borides are quite rare. A search in the literature reveals only a few boron-rich compounds such as $YSiB_{44}$ [1], $YSi_{4.6}B_{17.6}$ [2], $TbSi_{1.2}B_{41}$ [3], $RE_{1-x}Si_3B_{12}$ (RE = Y, Gd→Lu) [4,5] and $Tb_{3-x}C_2Si_8B_{36}$ [6], exhibiting icosahedral boron units. Attempts to establish isothermal sections from bulk materials and annealing of the samples at 1070 K have been performed for RE = Y, La, Ce, and Er, but no ternary phase has been mentioned [7,8]. Only small

*Corresponding author. Fax: +33 2 23 23 67 99.
E-mail address: roland.guerin@univ-rennes1.fr (R. Guérin).

0022-4596/$ - see front matter © 2005 Elsevier Inc. All rights reserved.
doi:10.1016/j.jssc.2005.02.023

solubility of boron has been noted in the RE_5Si_3 silicides (RE = Gd, Tb, Dy) [9] and recently for RE = Ce [10]. In order to extend this chemistry, we have decided to establish isothermal sections of some RE–Si–B phase diagrams at a higher temperature.

The isothermal section of the ternary Gd–Si–B diagram was tackled first at 1270 K from bulk experiments by X-ray diffraction (XRD), scanning electron microscopy and electron probe microanalysis. The choice of gadolinium was guided by the fact that it lies at the borderline between light and heavy rare-earth metals. The main feature of this diagram was the discovery of two ternary compounds, the Nowotny phase $Gd_5Si_3B_{0.64}$ which results from boron insertion in the binary compound Gd_5Si_3 of Mn_5Si_3 type, and $Gd_5Si_2B_8$, a new structural type resulting from the peritectic reaction between the solid GdB_4 and a liquid of composition Gd_5Si_3. Attention was turned next to other RE–Si–B diagrams (RE = Y, Nd, Dy, Ho, and Er) and the synthesis of the whole series of isostructural ternary compounds $RE_5Si_2B_8$ with different preparation techniques (arc melting, high-frequency furnace with the help of tantalum crucibles or even metal flux technique). The $RE_5Si_2B_8$ phase was observed for RE = Y, Sm→Ho, but not for light (RE = La→Nd) or heavy (RE = Er→Lu) rare-earth metals.

This paper deals with the crystal structures of all the members of the $RE_5Si_2B_8$ series (RE = Y, Sm, Gd, Tb, Dy, and Ho) as well as the magnetic and electrical properties for the terms with RE = Y, Gd, Tb, and Dy. A preliminary account of some of this work has been recently published [11,12]. Part of the present paper is devoted to the formation reaction of the phases and the comparison of the isothermal sections at 1270 K of some ternary phase diagrams (RE = Gd, Dy, and Ho). Finally, ^{11}B, ^{29}Si and ^{89}Y nuclear magnetic resonance (NMR) experiments have been performed on the nonmagnetic phase $Y_5Si_2B_8$. The local magnetic susceptibilities for $Y_5Si_2B_8$, deducted from ^{11}B NMR, are compared to those of the related binary YB_4, previously reported [13].

2. Experimental

Polycrystalline samples were prepared from pure elements: rare-earth metal as ingots (purity > 99.9%), silicon (> 99.99%) and boron (> 99%) as powders, all supplied by Strem Chemicals. Suitable amounts of powder and freshly filed chips of rare-earth metal were mixed together and pressed into pellets. Arc melting of the samples (800 mg each) was performed on a water-cooled copper hearth under a purified argon atmosphere with a Ti/Zr alloy as a getter. To ensure homogeneity, the samples were turned over and re-melted several times. In a second step, the as-cast samples were introduced in arc-welded sealed tantalum crucibles under 0.5 atm of argon, then heated up to 1850 K for 3 h with the help of a high-frequency furnace and finally slowly cooled to room temperature. This second annealing was necessary to improve the purity of the samples, especially for physical measurements. The molten buttons showed a metallic luster and were unreactive towards air. It can be noted that attempts to synthesize the phases by flux method, with tin, gallium or lead as a flux were always unsuccessful.

Platelet-shaped single crystals of all the ternary compounds $RE_5Si_2B_8$ (RE = Y, Sm, Gd, Tb, Dy, and Ho) were obtained by crushing the solidified samples. Energy dispersive spectroscopy and wavelength dispersive spectroscopy using scanning electron microscopy (Jeol JSM-6400) and electron microprobe analysis (Camebax SX 50) confirmed rare-earth metal, silicon, and boron as the only components in the samples [11]. A small part of each sample was pulverized and analysed by XRD using a powder diffractometer (CPS 120 INEL) equipped with a position-sensitive detector ranging 6–120° in 2θ.

Single-crystal intensity data for all the phases $RE_5Si_2B_8$ (RE = Y, Sm, Gd, Tb, Dy, and Ho) were collected at ambient temperature applying a Nonius Kappa CCD X-ray area-detector diffractometer with graphite-monochromatized Mo$K\alpha$ radiation ($\lambda = 0.71073$ Å). Data collection strategy was performed with the help of the program COLLECT [14] and reflections were corrected using the program DENZO of the Kappa CCD software package [15]. A numerical absorption correction was applied for RE = Tb, Dy and Ho on the basis of an optimized description of the crystal faces [16]. Structures were solved by direct methods (SIR 97) [17] and least-squares refinements, difference Fourier syntheses were run with SHELXL-97 [18] or JANA 2000 [19] program package. Experimental details and crystallographic data are summarized in Table 1. The program DIAMOND [21] was used for the drawings of the structural units.

The magnetic properties were studied by use of a Faraday balance (SUS 10) in the temperature range 80 K < T < 300 K and in external fields up to 1.3 T and a Lake Shore AC susceptometer (AC 7000, f = 133.3 Hz, B_{AC} = 1 mT) for temperatures 4.2 K ⩽ T ⩽ 100 K). The dc magnetization was measured in the temperature range 1.8–100 K and in fields up to 7 T using a superconducting quantum interference device magnetometer MPMS-XL (Quantum Design). Measurements of the electrical resistivity were carried out applying a common four-probe Lake Shore ac-resistivity option (f = 133.3 Hz, i = 10 mA) in the temperature range 4.2–300 K. The alloy buttons were cut into bars of approximately 1 mm^2 × 5 mm using a diamond saw (Bühler Isomet). Electrical contacts were made with commercial silver paint (Degussa, Hanau, Germany) and 25 μm gold wire.

Table 1
Crystal data, intensity collection and structure refinement for the $RE_5Si_2B_8$ compounds

Empirical formula	$Y_5Si_{1.87}B_8$[c]	$Sm_5Si_{1.82}B_8$	$Gd_5Si_{1.84}B_8$	$Tb_5Si_{1.88}B_8$	$Dy_5Si_{1.92}B_8$	$Ho_5Si_{1.94}B_8$
Molecular weight	583.26	889.35	924.42	933.91	955.16	967.31
Unit cell dimensions						
a (Å)	7.2234(2)	7.2616(3)	7.2665(3)	7.2320(2)	7.2209(2)	7.1830(2)
c (Å)	8.0961(3)	8.2260(3)	8.2229(7)	8.1263(4)	8.0545(3)	7.9900(3)
V (Å^3)	422.43(2)	433.76(3)	434.19(4)	425.02(3)	419.97(2)	412.25(2)
Calculated density (g/cm^3); Z	4.62; 2	6.85; 2	7.19; 2	7.32; 2	7.55; 2	7.79; 2
Crystal size (mm^3)	$0.036 \times 0.052 \times 0.052$	$0.13 \times 0.065 \times 0.02$	$0.02 \times 0.02 \times 0.017$	$0.07 \times 0.04 \times 0.01$	$0.085 \times 0.065 \times 0.025$	$0.03 \times 0.018 \times 0.014$
Linear absorption coefficient (mm^{-1})	34.17	33.51	37.85	41.26	44.13	47.63
Absorption coefficient (mm^{-1}) (T_{min}; T_{max})	—	—	—	0.132; 0.677	0.126; 0.371	0.363; 0.651
Absorption method	—	—	—	Analytical	Analytical	Analytical
Data collection						
θ range (°)	$4 \leqslant \theta \leqslant 35$	$2.5 \leqslant \theta \leqslant 27.4$	$2.5 \leqslant \theta \leqslant 26$	$2.5 \leqslant \theta \leqslant 31$	$2.5 \leqslant \theta \leqslant 32.5$	$2.5 \leqslant \theta \leqslant 40.2$
h	$-11 \leqslant h \leqslant 11$	$-9 \leqslant h \leqslant 9$	$-8 \leqslant h \leqslant 8$	$-10 \leqslant h \leqslant 10$	$-10 \leqslant h \leqslant 10$	$-12 \leqslant h \leqslant 13$
k	$-8 \leqslant k \leqslant 8$	$-6 \leqslant k \leqslant 6$	$-6 \leqslant k \leqslant 6$	$-8 \leqslant k \leqslant 10$	$-10 \leqslant k \leqslant 10$	$-13 \leqslant k \leqslant 10$
l	$-13 \leqslant l \leqslant 13$	$-10 \leqslant l \leqslant 10$	$-10 \leqslant l \leqslant 10$	$-10 \leqslant l \leqslant 11$	$-12 \leqslant l \leqslant 11$	$-12 \leqslant l \leqslant 14$
Refinement method	SHELXL; F^2	SHELXL; F^2	SHELXL; F^2	SHELXL; F^2	SHELXL; F^2	JANA; F
Reflections collected	1730[b]	928[b]	796[b]	4762	6569	8273
Independent reflections; R_{int}	534; 0.055	298; 0.045	260; 0.045	402; 0.058	446; 0.085	515; 0.076
Reflections in refinement ($I > 2\sigma(I)$)	436	279	228	362	426	464 ($I > 3\sigma\ (I)$)
Number of variables	28	28	28	28	28	28
Goodness-of-fit	1.08	1.09	1.06	1.03	1.08	1.02
R ($I > 2\sigma(I)$); wR_2 (or R_w[a])	0.040; 0.089	0.040; 0.098	0.041; 0.092	0.027; 0.065	0.026; 0.065	0.026; 0.040[a]
R (all data); wR_2 (or R_w[a])	0.051; 0.095	0.042; 0.100	0.047; 0.098	0.031; 0.066	0.028; 0.067	0.030; 0.042[a]
Extinction coefficient	0.0095(19); Shelxl	0.0037(7); Shelxl	0.0014(6); Shelxl	0.0027(4); Shelxl	0.0013(3); Shelxl	0.0044(18); B-C type I Lorentzian isotropic (Becker-Coppens, 1974)
$\Delta\rho$ (min, max) (e/Å^3)	−3.13; +2.52	−2.60; +3.54	-2.30; +3.65	−2.04; +3.74	−2.23; +3.61	−3.21; +3.23

[a and c]See also Ref. [20].

[b]Scaled and merged reflections.

The NMR spectra were recorded at ambient temperature either on a Chemagnetic Infinity 400 (^{11}B and ^{29}Si) or a Varian Infinity Plus 500 (^{89}Y) spectrometer under static and magic angle spinning (MAS) conditions. Several ^{11}B MAS NMR spectra were performed at different spinning speed at a frequency of 128.37 MHz, using a single pulse sequence. The chemical shifts are given with respect to external BF_3Et_2O [13]. ^{89}Y NMR experiments were carried out at 24.512 MHz, using a 7.5 mm MAS probe with low-gamma box. Spin echo rotor synchronized pulse sequences were employed with a recycling interval 40 s and 8000 transients. The spectra were referenced to $Y(NO_3)_3$ at 0 ppm, by taking $Y_2Ti_2O_7$ at 65 ppm as a secondary reference. ^{29}Si NMR static and MAS spectra were determined at 79.495 MHz. Spin echo pulse sequences were employed (rotor synchronized in case of MAS) with recycle interval of 0.2 s. ^{29}Si spectra were referenced to tetramethylsilane at 0 ppm, by using RTV at −22.3 ppm as a secondary reference.

3. Results and discussion

3.1. Experimental conditions of phase formation

Attempts to synthesize the ternary phase $RE_5Si_2B_8$, observed first with gadolinium, were carried out for all the other rare-earth metals. No phase could be obtained with the light rare-earth metals, i.e., La, Ce, Pr, and Nd. In contrast, $RE_5Si_2B_8$ phases were obtained with RE = Y, Sm, Gd, Tb, and Dy. The formation reaction of the ternary phase is the same for all rare-earth metals and results from a peritectic reaction between the binary REB_4 (solid) and a liquid of composition RE_5Si_3. This was proved through backscattered electron images upon constructing of the isothermal section of the Gd–Si–B phase diagram [11].

With RE = Ho, the ternary compound $Ho_5Si_2B_8$ could never be isolated as a pure phase. Only a few single crystals could be extracted from the molten sample and the X-ray powder pattern showed unambiguously that this phase is quite insignificant with respect to another ternary phase having the disordered AlB_2-type structure. The latter was in turn found to be the silicon-rich limit of the solid solution $HoB_{2-x}Si_x$ ($x\sim0.6$). Indeed, a comparison of the isothermal sections at 1270 K of both diagrams Gd–Si–B and Ho–Si–B, indicates that some essential differences occur on the boron side owing to the presence or the absence of the binary compound REB_2 (RE = Gd, and Ho) (Fig. 1). It turns out that GdB_2 is only formed above 1550 K whereas HoB_2 is stable at lower temperature. This means that in the case of holmium, there is a strong competition in the formation of both phases $Ho_5Si_2B_8$ and $HoB_{2-x}Si_x$ ($x\sim0.6$). Moreover, the solid solution $HoB_{2-x}Si_x$ when $x = 0.4$ almost includes $Ho_5Si_{\sim2}B_8$, i.e., $HoSi_{0.38}B_{1.6}$ in its composition range (Fig. 1b). A long re-annealing at 1270 K for more than 2 months in sealed silica tubes, did not lead to any modification of the composition of the initial mixture. As a consequence, this suggests that the temperature range for preparing the high-temperature phase $Ho_5Si_2B_8$ is probably very restricted. Similarly, the isothermal section of the ternary phase diagram Er–Si–B at 1270 K (not presented here) shows as well the occurrence of the solid solution $ErB_{2-x}Si_x$ ($x\sim0.6$). This was previously noticed by Chaban and Kuz'ma at 1070 K, but with a lower silicon content ($x = 0.15$) [8]. As mentioned above, the existence of the ternary compound $RE_5Si_2B_8$ requires a thermodynamic equilibrium with the binary phase REB_4. Unfortunately, this is not possible when the solid solution $REB_{2-x}Si_x$ is largely extended ($x\geqslant0.4$), as it is the case for erbium and probably for the other rare-earth metals Tm→Lu. This may explain why any attempt to synthesize ternary compounds $RE_5Si_2B_8$ with RE = Er→Lu was unsuccessful up to now. On the contrary, when RE = Dy, the solid solution $DyB_{2-x}Si_x$ is less extended ($x = 0.15$) and therefore the ternary phase $Dy_5Si_2B_8$ is observed (Fig. 1c).

3.2. Crystal structures

Each member of the $RE_5Si_2B_8$ series (RE = Y, Sm, Gd, Tb, Dy, and Ho) was structurally determined. From the intensity data set, the Laue symmetry $4/mmm$ was determined and according to the systematic extinctions $0kl$ ($k = 2n$) and $h00$ ($h = 2n$), the centrosymmetric space group $P4/mbm$ was chosen and found to be correct during structure determination. The atomic coordinates, displacement parameters and selected interatomic distances are given in Tables 2 and 3, respectively.

All the members of the $RE_5Si_2B_8$ series adopt the same structural arrangement with two crystallographically distinct rare-earth metal atoms ($RE1$ and $RE2$) and three types of boron atoms (B1, B2 and B3). The unique silicon position is not fully occupied (τ varies from 0.91 for Sm to 0.97 for Ho). The structure can simply be described as an intergrowth of ThB_4-like and U_3Si_2-like slabs of composition REB_4 and RE_3Si_2, respectively, which alternate along the [001] direction of the tetragonal unit cell (Fig. 2) [22,23]. It can then be considered as the topochemical sum $RE_5Si_2B_8 = 2REB_4 + RE_3Si_2$. A different coordination scheme is noted for the rare-earth metals with $RE1$ being octahedrally surrounded by two boron and four silicon atoms, and $RE2$ being in a rather complex 12-coordinated arrangement, made of nine boron and three silicon atoms.

Both boron and silicon substructures are independent and well ordered. The silicon atoms within the U_3Si_2-like slab form Si–Si pairs of ca. 2.35 Å, in accord with

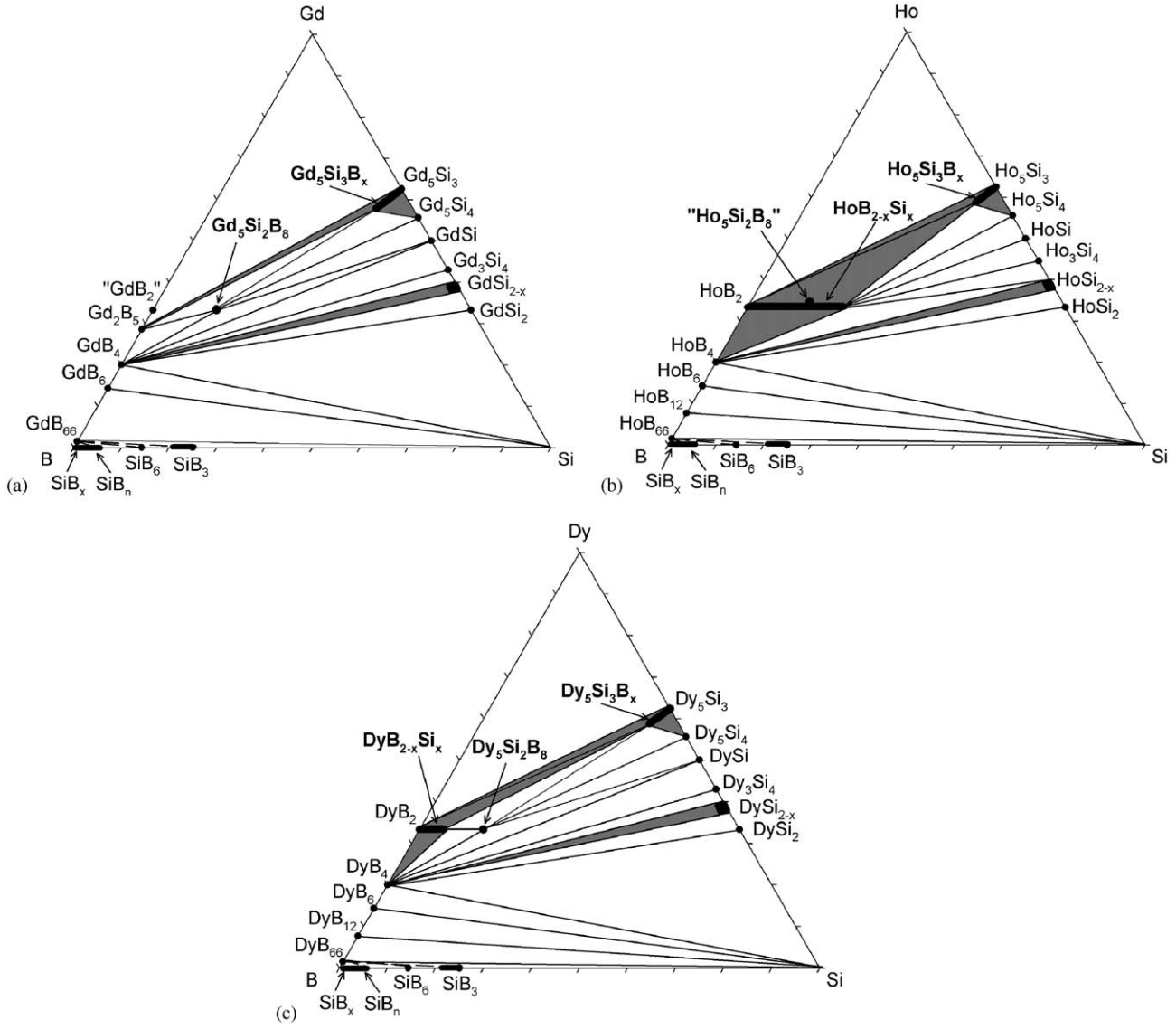

Fig. 1. Isothermal section of the phase diagrams at 1270 K: (a) Gd–Si–B, (b) Ho–Si–B, (c) Dy–Si–B. Axes are in at%. Two-phase regions are dashed in grey. For better understanding, GdB_2 and $Ho_5Si_2B_8$ are set in (a) and (b), respectively.

the ones of binary U_3Si_2 (2.30 Å) [23]. As shown in Table 3, the Si–Si distance slightly strengthens and converges towards the limiting value of ca. 2.34 Å, leading to a silicon covalent radius of 1.17 Å, in accord with Pauling's covalent radius scale [24].

The boron network within the ThB_4-like slab is two-dimensional made of squares and heptagons. Above and below the four basal B3 atoms, which form the squares, two apical B2 atoms are found leading to slightly distorted B_6 octahedra with nearly similar intra-octahedral B2–B3 and B3–B3 distances (Table 3). B1–B1 units connect four B_6 octahedra together in the *ab* plane through B1–B3 bonds. Being linked to one B1 and two B3 atoms, every B1 atom is three-connected and adopts a sp^2-type coordination mode with average bonding angles comprised between 123° (B3–B1–B1) and 113° (B3–B1–B3). It is worth mentioning that the B1–B1 units ($z = \frac{1}{2}$) and Si–Si pairs ($z = 0$) align on top of each other along the *c* direction. Comparing the B–B distances, we see that the mean B1–B3 and B1–B1 bond distances of 1.76 and 1.82 Å, respectively, are slightly shorter than the intra-octahedron distances which are ca. 1.85 Å. As it can be seen in Table 3, all B–B distances monotonically decrease from Sm to Ho, in accordance with the decrease of the metallic radius of the rare-earth metal [25]. As a consequence, the smallest distances are observed for holmium, for which the ternary phase is rather difficult to obtain (vide supra). The value of 1.74 Å for the covalent B1–B3 bond in $Ho_5Si_2B_8$, leading to a boron covalent radius of 0.87 Å, is in

Table 2
Atomic coordinates and isotropic displacement parameters for $RE_5Si_2B_8$ compounds

		Y	Sm	Gd	Tb	Dy	Ho
*RE*1	*x*	0	0	0	0	0	0
	y	0	0	0	0	0	0
	z	0	0	0	0	0	0
	U_{eq}	0.0110(2)	0.0178(5)	0.0201(6)	0.0130(2)	0.0079(2)	0.0083(2)
*RE*2	*x*	0.81897(4)	0.81902(7)	0.81899(7)	0.81884(4)	0.81887(3)	0.81879(3)
	y	0.68103(4)	0.68098(7)	0.68101(7)	0.68116(4)	0.68113(3)	0.68121(3)
	z	0.72410(6)	0.72455(8)	0.72480(12)	0.72475(6)	0.72528(4)	0.72557(4)
	U_{eq}	0.0074(2)	0.0071(4)	0.0107(5)	0.0061(2)	0.0060(2)	0.0053(2)
Si	*x*	0.3846(2)	0.3854(6)	0.3849(6)	0.3847(3)	0.3846(3)	0.3849(3)
	y	0.1154(2)	0.1146(6)	0.1151(6)	0.1153(3)	0.1154(3)	0.1151(3)
	z	0	0	0	0	0	0
	U_{eq}	0.0104(6)	0.0134(19)	0.0150(20)	0.0103(11)	0.0080(8)	0.0084(6)
	τ[a]	0.93(1)	0.91(2)	0.92(2)	0.94(2)	0.96(2)	0.97(2)
B1	*x*	0.9109(8)	0.9130(20)	0.9120(30)	0.9110(13)	0.9090(10)	0.9113(9)
	y	0.4109(8)	0.4130(20)	0.4120(30)	0.4110(13)	0.4090(10)	0.4113(9)
	z	0.5	0.5	0.5	0.5	0.5	0.5
	U_{eq}	0.0110(14)	0.010(4)	0.013(5)	0.007(2)	0.0041(16)	0.0055(16)
B2	*x*	0	0	0	0	0	0
	y	0	0	0	0	0	0
	z	0.3374(10)	0.3400(30)	0.3390(30)	0.3363(18)	0.3344(14)	0.3329(12)
	U_{eq}	0.0091(13)	0.0150(40)	0.0050(50)	0.0050(20)	0.0061(17)	0.0062(16)
B3	*x*	0.6724(7)	0.673(2)	0.6720(20)	0.6729(11)	0.6737(11)	0.6747(9)
	y	0.4597(8)	0.4600(2)	0.4610(30)	0.4606(13)	0.4606(11)	0.4605(11)
	z	0.5	0.5	0.5	0.5	0.5	0.5
	U_{eq}	0.0076(9)	0.011(3)	0.015(4)	0.0074(18)	0.0079(17)	0.0070(17)

[a]Occupancy factors with their esd's.

Table 3
Interatomic distances (Å) with their esd's for $RE_5Si_2B_8$ compounds

		Y	Sm	Gd	Tb	Dy	Ho
*RE*1	2B2	2.732(8)	2.79(2)	2.78(3)	2.732(14)	2.694311)	2.660(10)
	4Si	2.900(1)	2.919(3)	2.919(3)	2.905(2)	2.900(2)	2.886(2)
*RE*2	2B3	2.640(4)	2.664(12)	2.667(13)	2.644(6)	2.632(6)	2.614(5)
	2B2	2.696(2)	2.715(4)	2.716(5)	2.698(3)	2.691(2)	2.676(2)
	2B3	2.711(4)	2.745(12)	2.748(15)	2.725(7)	2.715(6)	2.697(6)
	2B1	2.746(3)	2.768(7)	2.778(9)	2.756(4)	2.753(3)	2.730(5)
	B1	2.967(7)	3.016(17)	3.010(20)	2.977(10)	2.951(8)	2.951(5)
	Si1	3.052(2)	3.089(4)	3.086(4)	3.056(2)	3.036(2)	3.015(2)
	2Si1	3.130(1)	3.158(2)	3.159(2)	3.135(2)	3.115(2)	3.092(2)
Si	Si	2.358(4)	2.355(13)	2.365(13)	2.358(7)	2.357(6)	2.338(3)
B1	2B3	1.758(7)	1.776(18)	1.78(2)	1.759(10)	1.739(9)	1.736(9)
	B1	1.821(17)	1.79(4)	1.81(5)	1.82(3)	1.86(2)	1.802(10)
B2	4B3	1.835(7)	1.845(19)	1.85(2)	1.848(12)	1.853(10)	1.854(8)
B3	B1	1.758(7)	1.776(18)	1.78(2)	1.759(10)	1.739(9)	1.736(9)
	2B3	1.809(7)	1.82(2)	1.82(2)	1.814(12)	1.819(11)	1.819(10)
	2B2	1.835(7)	1.845(19)	1.85(2)	1.848(12)	1.853(10)	1.854(8)

agreement with literature for a covalent single bond [24]. This distance is also found in the dysprosium-containing compound, meaning that this is the limit value for a B–B single bond, which is necessary for stabilizing the ternary phases $RE_5Si_2B_8$. Therefore, this may explain why the corresponding erbium compound could not be

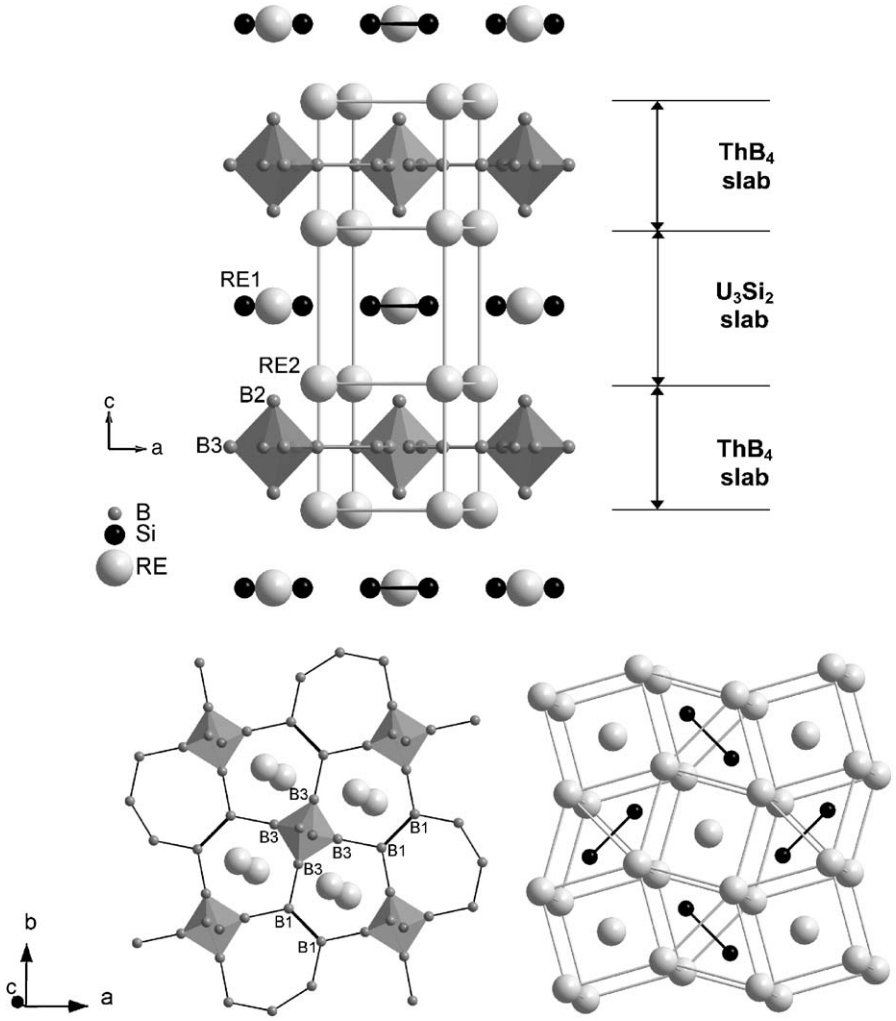

Fig. 2. Crystal structure of the $RE_5Si_2B_8$ compound: 3D representation showing the ThB_4-like and U_3Si_2-like slabs, along the [001] direction (top) and a view of the ThB_4- and U_3Si_2-like slabs down to the c axis (bottom).

synthesized. Of course, the competition between both ternary phases $RE_5Si_2B_8$ and $REB_{2-x}Si_x$ for $RE = Er \rightarrow Lu$ is quite important and, from a bonding point of view, in favour of the disordered AlB_2-type structure. For this purpose, the single-crystal structure of the phase $HoB_{2-x}Si_x$ ($x = 0.6$) has been determined: hexagonal symmetry, unit cell parameters $a = 3.4078(2)$ Å and $c = 3.9849(4)$ Å, $P6/mmm$ space group, $R = 0.010$, $R_w = 0.016$, GOF = 1.085, 73 unique reflections with $I > 2\sigma(I)$, seven variable parameters, holmium and mixed (B, Si) atoms in *1a* and *2d* positions, respectively. Boron occupies 70 at% of the mixed position in this structure, and the metalloid–metalloid distance is 1.967(1) Å, which is largely higher than the smallest one measured in the $Ho_5Si_2B_8$ structure. It is worth noting that in the case of the binary compound HoB_2 of AlB_2 type, the corresponding boron–boron distances are 1.894(1) Å, whereas in the case of $HoSi_{2-x}$ ($x \sim 0.4$) of AlB_2-type, the Si–Si distance is equal to 2.199(1) Å.

3.3. Magnetic and electrical properties

The physical properties have been measured on the ternary compounds $RE_5Si_2B_8$ with $RE = Y$, Gd, Tb, and Dy. No study has been done with samarium since the ternary compound $Sm_5Si_2B_8$ occurs but only as a minor phase in corresponding samples. In the case of holmium, only a few single crystals of the ternary phase could be obtained (vide supra).

The results of the magnetic and electrical resistivity measurements for the compounds $RE_5Si_2B_8$ ($RE = Y$, Gd, Tb, and Dy) are summarized in Figs. 3–8. $Y_5Si_2B_8$ is a Pauli-type paramagnet and the susceptibility remains practically temperature independent down to 10 K. An increase of χ (Curie tail) down to 1.8 K is due to small amounts of impurity phases. For the compounds $RE_5Si_2B_8$ ($RE = Gd$, Tb, and Dy), the reciprocal susceptibilities obey the linear Curie–Weiss law as it can be seen in Fig. 3. The values of the effective

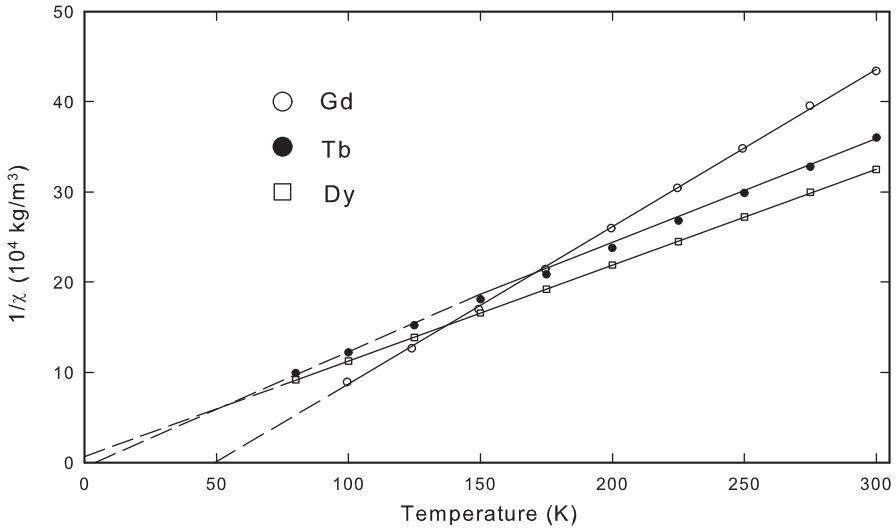

Fig. 3. Reciprocal susceptibility versus temperature for $RE_5Si_2B_8$ (RE = Gd, Tb, and Dy). Solid line fitted after Eq. (1).

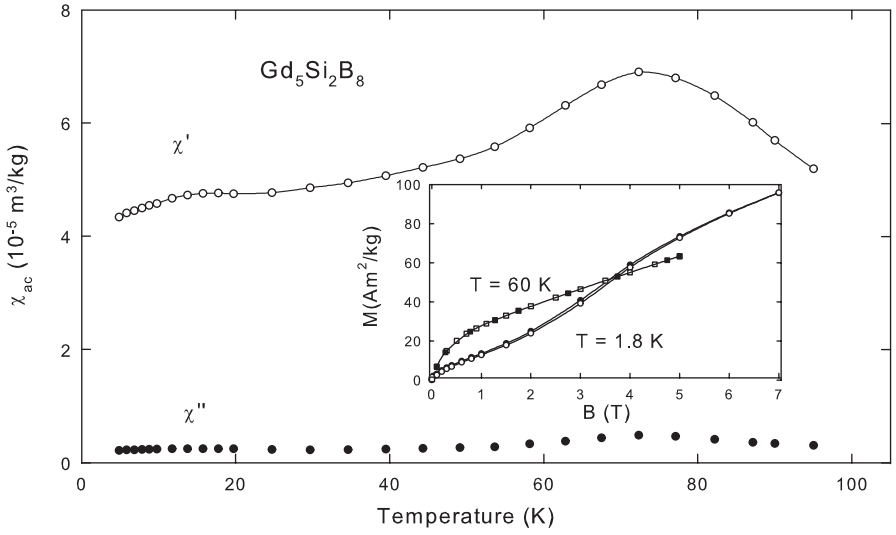

Fig. 4. Dynamic susceptibilities versus temperature for $Gd_5Si_2B_8$. Inset: magnetization versus field at $T = 60$ and 1.8 K (open/filled symbols in increasing/decreasing field).

magnetic moments together with the paramagnetic Curie temperatures were calculated by least squares fits using the modified formula

$$\chi = \frac{C}{T - \Theta_p} + \chi_0, \quad (1)$$

C being the Curie constant, Θ_p is the paramagnetic Curie temperature and χ_0 denotes temperature-independent contributions such as core diamagnetism, Landau diamagnetism and Pauli paramagnetism. The effective moments, listed in Table 4, are in good accordance with the theoretical tripositive ion moments.

In general, the low-temperature magnetic behavior of these compounds is rather similar. As shown in Figs. 4–6, the *dc* and the real parts of the *ac* susceptibilities are characterized by the occurrence of pronounced maxima due to the onset of antiferromagnetic ordering of the rare-earth atoms. In the case of the Gd-containing compound (Fig. 4), which was reported earlier [12], a peculiar magnetic situation was suggested. Obviously, at T_{max} which corresponds to 70 K, the nature of the ordering is a canted ferromagnetism, which is proved by the isothermal magnetization curve at $T = 60$ K (see inset Fig. 4). The canting angle of the moments was estimated to reach 15° at 5 T. Below the Néel temperature, which was derived from electrical resistivity measurements, i.e., $T_N = 44$ K (vide infra), the canting of the moments is suspended and a linear field dependence of the magnetization in moderate

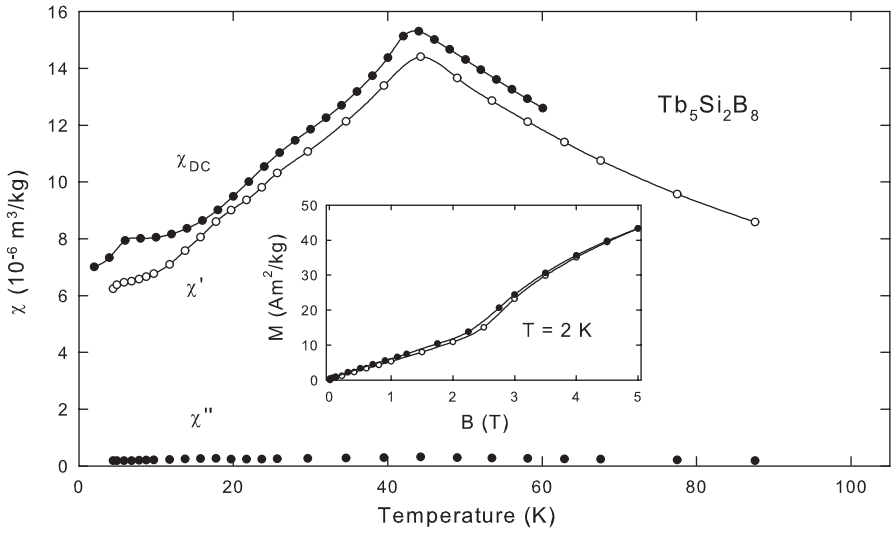

Fig. 5. Static and dynamic susceptibilities versus temperature for $Tb_5Si_2B_8$. Inset: magnetization versus field at $T = 2\,K$ (open/filled symbols in increasing/decreasing field).

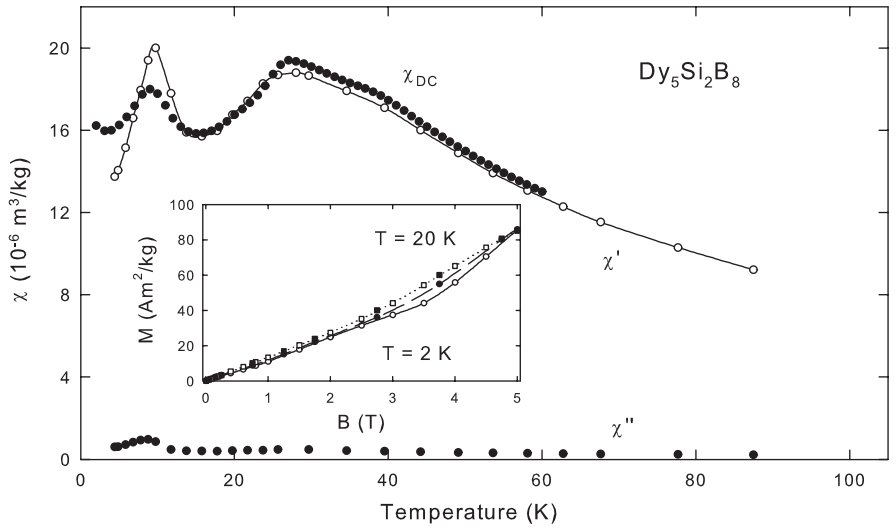

Fig. 6. Static and dynamic susceptibilities versus temperature for $Dy_5Si_2B_8$. Inset: magnetization versus field at $T = 20$ and 2 K (open/filled symbols in increasing/decreasing field).

fields is observed at $T = 1.8\,K$. Above a critical field of $B = 2\,T$, a metamagnetic-like transition sets in. However, even at 7 T, only a reduced order moment of $3.3\,\mu_B$/Gd atom was derived, far below the saturation moment of $7\,\mu_B$, indicating an increase of the canting angle to about 30°. This interpretation of the experimental findings is furthermore supported by the weak temperature dependence of the imaginary part of the *ac* susceptibility curve in the temperature interval $50\,K < T < 80\,K$ in the ferromagnetic state and by an independence of the temperature below 50 K due to an antiparallel spin alignment. The relatively large and positive value of Θ_p seems to be in accord with this assumption also.

The magnetic data of the compound $Tb_5Si_2B_8$ presented in Fig. 5 corroborate with an antiferromagnetic ordering ($T_N = 45\,K$). The isothermal magnetization curve at $T = 2\,K$, which is fully reversible, again proves a metamagnetic transition above $B = 3\,T$ (inset Fig. 5). The ordered moment of $1.4\,\mu_B$/Tb atom at the maximum field is well below the saturation value. In order to get a solution of the magnetic structure, we shall prepare a sample with B^{11} for neutron diffraction experiments.

The compound $Dy_5Si_2B_8$ undergoes also an antiferromagnetic transition at $T_N = 28\,K$ (Fig. 6). At $T_C = 10\,K$, a second but ferromagnetic transition is

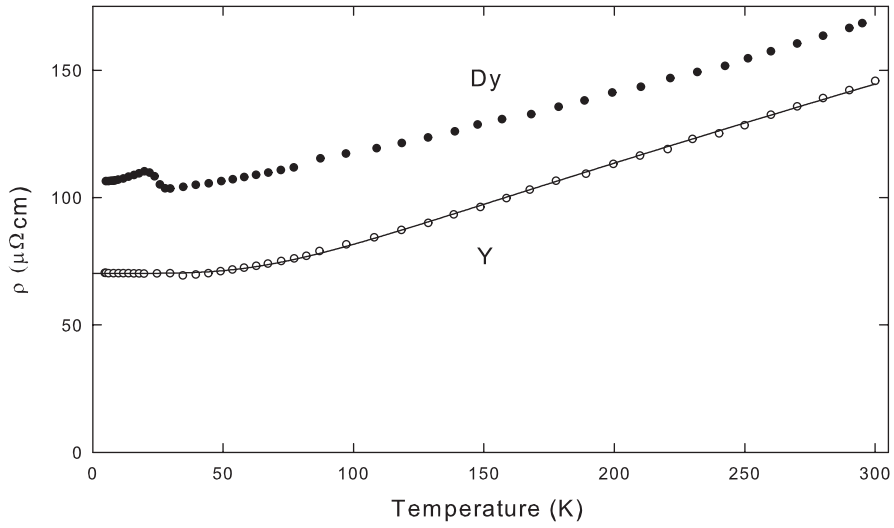

Fig. 7. Electrical resistivity versus temperature for $RE_5Si_2B_8$ compounds (RE = Y, and Dy). Solid line calculated according to Eq. (2).

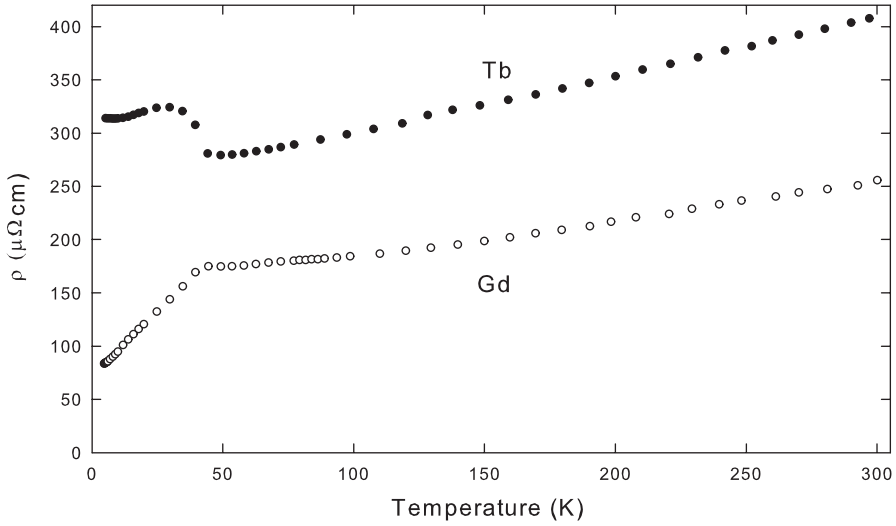

Fig. 8. Electrical resistivity versus temperature for $RE_5Si_2B_8$ compounds (RE = Gd, and Tb).

Table 4
Magnetic and electrical resistivity data for ternary compounds $RE_5Si_2B_8$

Compound	μ_{eff} (μ_B)	Θ_p (K)	T_C (K)	T_N (K)	$(d\rho/dT)_{max}$ (K)
$Y_5Si_2B_8$	$\chi_{(300\,K)} = 1.5 \times 10^{-8}\,m_3/kg$, $\chi_{(1.8\,K)} = 8 \times 10^{-7}\,m^3/kg$				
$Gd_5Si_2B_8$	8.2	50	70	44	72, 44
$Tb_5Si_2B_8$	9.9	4	—	45	46
$Dy_5Si_2B_8$	10.7	−6	—	28	29

observed. However, looking at the isothermal magnetization versus field (inset Fig. 6) for two distinct temperatures, $T = 20$ and 2 K, a linear dependence of $M(B)$ up to $B = 3.5$ T is followed by an upturn due to a metamagnetic transition. Hence we tend to believe that the ferromagnetic transition is not an intrinsic behavior of this sample, but rather stems from a small amount of a secondary phase (e.g., $DyB_{2-x}Si_x$). Such an assumption should also explain the observed weak hysteresis at elevated external fields at $T = 2$ K.

The results of the electrical resistivity versus temperature for the samples $RE_5Si_2B_8$ are presented for $RE = Y$, and Dy in Fig. 7 and for $RE = Gd$, and Tb in Fig. 8. The $\rho(T)$ curve for $Y_5Si_2B_8$ resembles the typical shape of a metal-like intermetallic compound. Assuming the validity of Mathiesen's rule, the resistivity of a nonmagnetic compound follows the Bloch–Grüneisen relation [26,27]:

$$\rho(T) = \rho_0 + 4R\Theta_D\left(\frac{T}{\Theta_D}\right)^5 \int_0^{\Theta_D/T} \frac{x^5\,dx}{(e^x - 1)(1 - e^{-x})}. \quad (2)$$

We have fitted our data according Eq. (2) with the following results: residual resistivity ($\rho_0 = 70\,\mu\Omega\,cm$), the second phonon scattering term ρ_{ph} ($R = 0.28\,\mu\Omega\,cm/K$; the Debye temperature $\Theta_D = 433\,K$.

The resistivities of $RE_5Si_2B_8$ ($RE = Gd$, Tb, and Dy) decrease below room temperature due to the metallic state. In the low-temperature regime, we observe the typical changes of slope owing to the onset of magnetic order, which corresponds to ordering temperatures described above, as well as pronounced negative temperature coefficients of $\rho(T)$ resulting from superzone scattering [28]. The maxima of the derivatives $d\rho/dT$ as listed in Table 4 are in good agreement with the ordering temperatures derived from magnetic data.

3.4. NMR experiments

^{11}B ($I = 3/2$), ^{29}Si ($I = 1/2$) and ^{89}Y ($I = 1/2$) MAS and static NMR experiments were carried out on nonmagnetic $Y_5Si_2B_8$. Indeed, NMR experiments are usually difficult to perform with electronic conductors and strongly paramagnetic compounds, as are most of the members of the $RE_5Si_2B_8$ series. $Y_5Si_2B_8$ does not present any localized magnetic moment and therefore is the best candidate for NMR Knight shift measurements. As said above, the $Y_5Si_2B_8$ structure can be described as an intergrowth structure built from alternating YB_4 and Y_3Si_2 slabs along the [001] direction. The ^{11}B NMR spectroscopy has been used to characterize the local Pauli spin susceptibility on the boron sites in $Y_5Si_2B_8$, in order to compare with the ^{11}B NMR results for the related compound YB_4, recently proposed by B. Jäger et al. [13].

The Knight shift (K) of ^{11}B NMR is usually decomposed into three components, each of them directly related to the different contributions to the bulk magnetic susceptibility [29]. The first one is a Fermi contact term, which contributes to the K in two ways, i.e., a direct contribution related to the density of states of s-like wave functions at the Fermi level and an indirect one, via a polarization of electrons below the Fermi level. The second contribution is a dipolar interaction term between nuclear and electronic spins and the last one corresponds to a term analogous to the Van Vleck contribution to the magnetic susceptibility. Fig. 9a represents an 8 kHz MAS NMR spectrum recorded using a rotor-synchronized spin-echo pulse sequence. The spectrum, obtained by Fourier transformation of the second half of the echo only, is the result of averaging 256 transients with a recycle interval of 2 s.

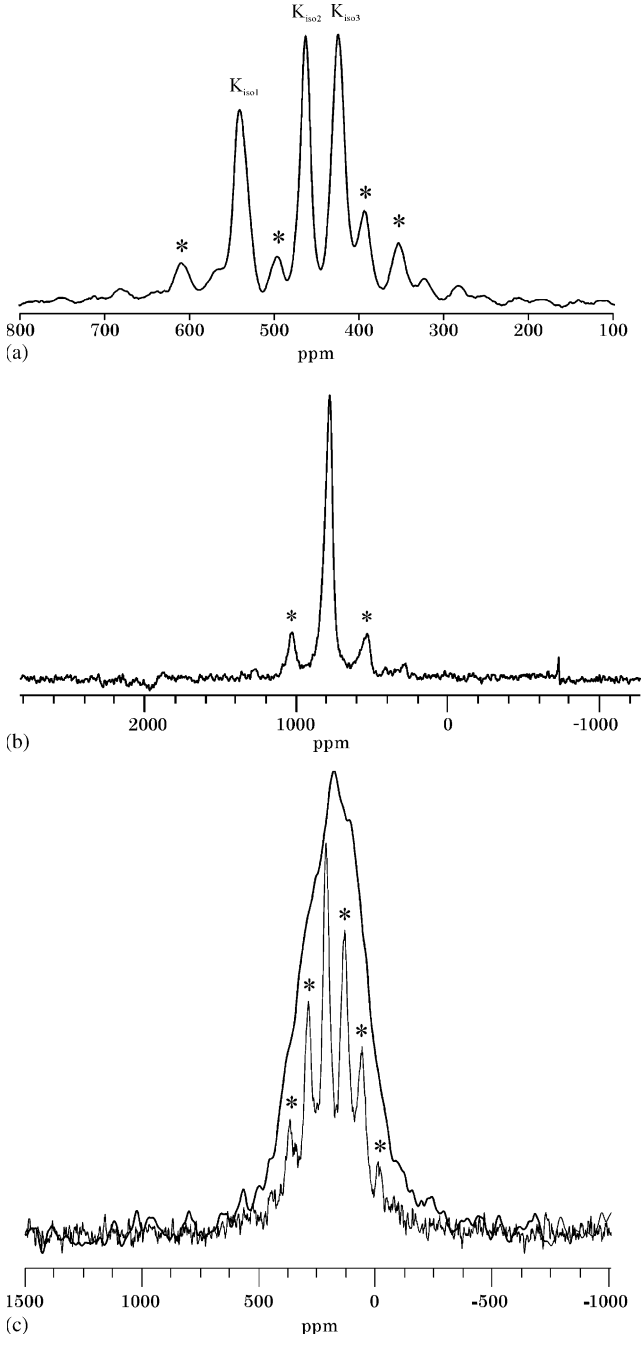

Fig. 9. Solid-state NMR spectra for $Y_5Si_2B_8$: (a) ^{11}B MAS recorded with a MAS rate of 8 kHz. The three ^{11}B NMR isotropic Knight shift resonances are labelled K_{iso1}, K_{iso2}, and K_{iso3}, (b) ^{89}Y MAS recorded with a MAS rate of 8 kHz, (c) static spectrum and ^{29}Si MAS recorded with a MAS rate of 6.125 kHz. The positions of spinning sidebands are indicated by *.

The lineshape is clearly dominated by Knight shift anisotropies and does not show any distinctive feature of quadrupolar effects (either first or second order). The MAS spectra at different spinning speeds allow to separate three isotropic Knight shift values at $K = 538$, 462 and 425 ppm, respectively. The three signals are consistent with the three crystallographically distinct boron sites in the structure. The overlapping spinning sidebands hinder the analysis of the different Knight shift anisotropies. The ^{11}B NMR lineshapes for $Y_5Si_2B_8$ are not dominated by first-order quadrupolar interactions, unlike those observed for YB_4 and YB_6 by Jäger et al. [13]. ^{11}B shifts in $Y_5Si_2B_8$ are found to be largely higher than the ones in the binary YB_4 ($K = -1$ ppm for all sites), but are of the same order of magnitude than the K values in YNi_2B_2C ($\approx$400 ppm) [30]. The ^{11}B NMR experiments exhibit substantially different electronic properties for the YB_4 slabs in the binary YB_4 and in the ternary $Y_5Si_2B_8$. It is worth noting that the boron layers are fully independent in the ternary while they are linked by B–B bonds (1.63 Å) in the binary, through neighbouring octahedra [31]. As proposed for YB_4, the main contribution to the ^{11}B Knight shift can presumably be attributed to *s*-type density of states at the Fermi level. The much higher ^{11}B Knight shifts for $Y_5Si_2B_8$ are indicative of a significantly higher density of states at the Fermi level on the boron sites for *s*-type wave functions. Preliminary theoretical calculations on $Y_5Si_2B_8$ and YB_4 seem to corroborate this hypothesis [32].

^{89}Y MAS spectrum on $Y_5Si_2B_8$ is shown in Fig. 9b. The MAS spectrum exhibits two clear spinning sidebands and one asymmetric main peak at about 800 ppm. The asymmetry can be explained by two ^{89}Y NMR signals, which correspond to the two nonequivalent yttrium crystallographic sites. The poor resolution is due to the metallic behavior of the compound and therefore hinders the separation of the two signals. In the absence in literature of ^{89}Y NMR data for YB_4, no comparative study between $Y_5Si_2B_8$ and YB_4 (only one yttrium crystallographic site) can be presently established. The large positive shifts (about 800 ppm) are consistent with the ones for yttrium hydrides, given by several authors [33,34].

^{29}Si NMR MAS and static spectra are presented in Fig. 9c. The static spectrum shows a strong Knight shift anisotropy of about 600 ppm. The MAS spectrum indicates a single silicon site and a strong isotropic K value of 217 ppm. There is no NMR evidence of silicon deficiency as found by XRD study.

4. Conclusion

We have studied the structural and physical properties (magnetism, electrical transport, NMR spectroscopy) of the ternary rare-earth metal silicide borides $RE_5Si_2B_8$. Part of our work has been devoted to the formation reaction of the phases with the description of the isothermal sections of the ternary phase diagrams *RE*–Si–B at 1270 K (*RE* = Gd, Dy, and Ho). Their crystal structure can simply be described as an intergrowth of two building slabs REB_4 and RE_3Si_2 of the ThB_4 and U_3Si_2 types, respectively, which alternate along the *c*-axis of the tetragonal unit cell. Both silicon and boron substructures are wholly independent and well ordered.

Magnetic and electrical properties have been carried out on samples containing Gd, Tb, Dy, and Y. Except $Y_5Si_2B_8$, which is a Pauli-independent paramagnet, the three other phases order antiferromagnetically at a Néel temperature of $T_N = 44$ K (Gd), 45 K (Tb) and 28 K (Dy). It is worth noting that the corresponding rare-earth metal tetraborides REB_4 show also antiferromagnetic ordering with Néel temperatures very close to those of the silicide borides [35–37]. Consequently, one can conclude that the REB_4 slabs are dominating the magnetic order in the ternary phases $RE_5Si_2B_8$. In order to check this assumption, future investigations on the magnetic structure of $Tb_5Si_2B_8$ by neutron diffraction experiments will be performed.

^{11}B, ^{29}Si and ^{89}Y NMR spectroscopy confirm the number of boron, silicon and yttrium sites found in the structure from XRD analysis. Comparison of the ^{11}B NMR data of $Y_5Si_2B_8$ to those of YB_4 indicates a substantial difference of the local magnetic susceptibilities in the YB_4 slabs for the two compounds. XRD studies and bulk magnetic susceptibilities suggest that the structure can be described as a stacking of independent YB_4 and Y_3Si_2 slabs. However, the variation of the electronic properties encountered by ^{11}B solid-state NMR between YB_4 and $Y_5Si_2B_8$ tends to prove that these slabs interact together.

5. Supporting information available

Further details on the crystal structure investigations may be obtained from the Fachinformationszentrum Karlsruhe, 76344 Eggenstein-Leopoldshafen, Germany (fax: (49) 7247-808-666; e-mail: crysdata@fiz.karlsruhe.de), on quoting the depository numbers CSD-414567 (Y), CSD-414568 (Tb), CSD-414569 (Sm), CSD-414570 (Ho), CSD-414571 (Gd), and CSD-414572 (Dy).

Acknowledgments

V. Babizhetskyy is grateful to the Centre National de la Recherche Scientifique (France) for a research grant (2001–2002). The authors also thank T. Roisnel (CDIFX, Université de Rennes 1) for X-ray intensity data collection as well as J.C. Jégaden, J. Le Lannic

(CMEBA, Université de Rennes 1), and M. Bohn (IFREMER, Brest) for their assistance in SEM and EPMA studies. Dr. I. Farnan (Department of Earth Sciences, University of Cambridge, UK) is acknowledged for access to solid-state NMR facilities. This research was partly supported by the Austrian (ÖAD)–French (Foreign Affairs Ministry)–Amadeus 2002–2003 exchange program (Projects 10/2002 (Austria), 00064 K and 0376XJ (France)).

References

[1] I. Higashi, T. Tanaka, K. Kobayashi, Y. Ishizawa, M. Takami, J. Solid State Chem. 133 (1997) 11.
[2] F.X. Zhang, A. Sato, T. Tanaka, J. Solid State Chem. 164 (2002) 361.
[3] T. Mori, T. Tanaka, J. Solid State Chem. 154 (2000) 223.
[4] F.X. Zhang, F.F. Xu, T. Mori, Q.L. Liu, T. Tanaka, J. Solid State Chem. 170 (2003) 75.
[5] F.X. Zhang, T. Tanaka, Z. Kristallogr. 218 (2003) 26.
[6] J.R. Salvador, D. Bilc, S.D. Mahanti, M.G. Kanatzidis, Angew. Chem. Int. Ed. 41 (2002) 844.
[7] Yu.B. Kuz'ma, N.F. Chaban, Binary and Ternary Systems Containing Boron, Metallurgiya, Moscow, 1990.
[8] N.F. Chaban, Yu.B. Kuz'ma, Inorg. Mater. 36 (2000) 882.
[9] I. Mayer, I. Felner, J. Less-Common Met. 37 (1974) 171.
[10] R. Jardin, F. Weitzer, J. Bauer, K. Hiebl, J. Alloys Compds. 359 (2003) 35.
[11] V. Babizhetskyy, J. Roger, S. Députier, R. Jardin, J. Bauer, R. Guérin, J. Solid State Chem. 177 (2004) 415.
[12] V. Babizhetskyy, J. Roger, S. Députier, R. Guérin, R. Jardin, J. Bauer, K. Hiebl, C. Jardin, J.-Y. Saillard, J.-F. Halet, Angew. Chem. Int. Ed. 43 (2004) 1979.
[13] B. Jäger, S. Paluch, W. Wolf, P. Herzig, O.J. Zogal, N. Shitsevalova, Y. Paderno, J. Alloys Compds. 383 (2004) 232.
[14] COLLECT: KappaCCD software, Nonius BV, Delft, The Netherlands, 1998.
[15] Z. Otwinowski, W. Minor, in: C.W. Carter Jr., R.M. Sweet (Eds.), Methods in Enzymology, vol. 276, Academic Press, New York, 1997, p. 307.
[16] J. de Meulenaar, H. Tompa, Acta Crystallogr. A 19 (1965) 1014.
[17] A. Altomare, M.C. Burla, M. Camalli, B. Carrozzini, G.L. Cascarano, C. Giacovazzo, A. Guagliardi, A.G.G. Moliterni, G. Polidori, R. Rizzi, Acta Crystallogr. A 32 (1999) 115.
[18] G.M. Sheldrick, SHELXL-97, Program for the Refinement of Crystal Structures, University of Göttingen, Germany, 1997.
[19] V. Petricek, M. Dusek, JANA 2000, Crystallographic Computing System for Ordinary and Modulated Structures, Institute of Physics, Academy of Sciences of the Czech Republic, Praha, 2000.
[20] J. Roger, R. Jardin, V. Babizhetskyy, S. Députier, J. Bauer, R. Guérin, Z. Kristallogr. NCS 218 (2003) 173.
[21] K. Brandenburg, Diamond, Version 2.0, 1998.
[22] A. Zalkin, D.H. Templeton, Acta Crystallogr. 6 (1953) 269.
[23] K. Remschnig, T. Le Bihan, H. Noël, P. Rogl, J. Solid State Chem. 97 (1992) 391.
[24] L. Pauling, Nature of the Chemical Bond, third ed, Cornell University Press, Ithaca, NY, 1960.
[25] F. Laves, Theory of Alloys Phases, ASM, Cleveland, OH, 1956.
[26] N.F. Mott, H. Jones, Theory of the Properties of Metals and Alloys, Oxford University Press, London, 1964.
[27] G. Grimvall, The Electron–Phonon Interaction in Metals, North-Holland, Amsterdam, 1981.
[28] G.T. Meaden, Contemp. Phys. 12 (1971) 313.
[29] H. Ebert, J. Abart, J. Voitländer, J. Phys. F 16 (1986) 1287.
[30] B.J. Suh, F. Borsa, D.R. Torgeson, B.K. Cho, P.C. Canfield, D.C. Johnson, J.Y. Rhee, B.N. Harmon, Phys. Rev. B 54 (1996) 15341.
[31] A. Guette, M. Vlasse, J. Etourneau, R. Naslain, C.R. Acad. Sci. Paris, Ser. C 291 (1980) 145.
[32] M. Ben Yahia, R. Gautier, J.-Y. Saillard, J.-F. Halet, Unpublished results.
[33] X. Helluy, J. Kummerlen, A. Sebald, O.J. Zogal, Solid State NMR 14 (1999) 225.
[34] R.G. Barnes, D.R. Torgeson, T.J.M. Bastow, G.W. West, E.F.W. Seymour, M.E. Smith, Z. Phys. Chem. Neue Folge 164 (1989) S867.
[35] G. Will, W. Schaefer, F. Pfeiffer, F. Elf, J. Etourneau, J. Less-Common Met. 82 (1981) 349.
[36] G. Will, W. Schaefer, J. Less-Common Met. 67 (1979) 31.
[37] F. Elf, W. Schaefer, G. Will, J. Etourneau, Solid State Commun. 40 (1981) 579.